



Modelling and Experimental Characterization of Processing Parameters in Vertical Twin Roll Casting of Aluminium Alloy A356

B. Dhindaw ^{a,*}, S. Singh ^b, A. Mandal ^b, A. Pandey ^b

^a Indian Institute of Technology Bhubaneswar/Kharagpur, India

^b Indian Institute of Technology Bhubaneswar, India

* Corresponding author: Email address: dhindaw@gmail.com

Received 05.08.2020; accepted in revised form 13.11.2020

Abstract

Production of near net shape thin strips using vertical twin roll casting method has been studied. In a typical VTRC process, the simultaneous action of solidification and rolling makes the process quite attractive as well as complicated. An industrially popular alloy A356 has been chosen for the VTRC processing. It is challenging to identify VTRC processing parameters for the alloy to produce thin strips because of its freezing range and complex composition. In the present work processing parameters of VTRC like roll speed, roll gap, melt superheat and the interface convective heat transfer coefficient have been investigated through modelling of the process. The mathematical model was developed which simultaneously solves the heat transfer, fluid flow and solidification, using commercial software COMSOL Multiphysics 5.4. VTRC sheets of alloy A356 were produced in an experimental set up and attempts were made to correlate the microstructures of VTRC A356 alloy to that predicted from the numerical studies to validate the model.

Keywords: Aluminium alloy A356, Structural materials, Numerical modelling, Vertical twin-roll casting

1. Introduction

A356 is a cast Aluminium alloy with the major alloying elements as 7% Si and 0.3% Mg along with minor alloying elements as 0.2% Fe (max) and 0.10% Zn (max) [1, 2]. Addition of Si enhances the fluidity of the material in the molten stage which helps in preventing the premature solidification and thereby enhances the castability of material and reducing the chances of hot-tearing/hot-cracking. Excellent castability makes it a logical choice for intricate and complex castings where lightweight and excellent mechanical properties are the important factor. Due to their high specific strength, stiffness, low density, and excellent

casting properties this alloy is globally applicable in automobiles and aerospace industries. Despite having all these favourable conditions, the morphology of eutectic-Si limits the application of this alloy. The microstructure of A356 is characterized by soft primary α -Al phase growing as dendrite with hard and brittle eutectic (α -Al+Si) phase formed in the interdendritic region along with the other intermetallic phases such as Mg_2Si , α - $Al_{15}(FeMn)_3Si_2$ and β - Al_5FeSi . The acicular morphology of eutectic-Si tends to act as stress raiser and leads to the crack propagation. This reduces the ductility and toughness of the cast products. A suitable processing route is required to change the morphology of eutectic-Si particles and to refine the grain size of

primary α -Al dendrites. One of the thermo-mechanical processes used for microstructural modification is vertical twin-roll casting process (VTRC). VTRC is primarily used for production of thin sheets (1-6 mm). This process is an advance continuous casting process which combines both casting and marginal hot rolling simultaneously to produce near-net shape castings in a single step [3].

Conventional DC casting is used for production of cylindrical billets or rectangular ingots/blooms of 200-300 mm thickness [4-5]. These slabs/ingots/blooms are further processed to obtain sheets of desired thickness. The production cost for sheets manufactured using this process is comparatively higher than the VTRC process as it involves many intermediate heating and rolling steps to obtain the minimum thickness of a sheet. This process is not economical for small-batch production, while VTRC can be used for both small and mass production. VTRC is energy efficient process requires less space and it helps in reducing up to 80% greenhouse gas emission as compared to the DC casting [6]. In addition VTRC provides very high cooling rate (10^2 - 10^3 K/sec) with large rolling force which helps in providing a significant change in the morphology of eutectic-Si.

The concept of continuous casting in a single stage was first developed by Bessemer, in 1857, who envisioned a twin-roll casting (TRC) technique to cast steel strips. TRC is a sustainable manufacturing technology to produce sheets directly from liquid molten metal in less time with refined microstructure [7], but some defects such as shrinkage porosity, centreline-segregation and surface bleed are observed during sheet production by TRC process. Surface bleeds caused because of incomplete solidification before reaching to the nip point (minimum distance between two rolls) was mostly observed during casting of hypereutectic Al-Si alloys, which possess high flow-ability in semisolid condition. Experiments were performed by increasing the roll diameter but no significant reduction in surface bleed defect has been obtained. Many studies suggest that these defects can be reduced by controlling the processing parameters involved during VTRC process. The roll speed, roll gap, melt superheat and convective heat transfer coefficient between roll surface and solidifying material are the four main parameters that directly affect the sheet quality. N.S Barekar et al. [8], studied the literature on process aspect, modelling and quality issues for various aluminium alloys. The role of process parameters on solidification during casting was also reviewed. It is found that optimization of these parameters was necessary to minimize these defects and to increase the sheet production to meet increasing demand. TRC involves complex fluid flow, solidification and heat transfer. Hence, computational analysis is a suitable tool for understanding of this process. Computational analysis is a cost-effective way to optimize the process parameters as it reduces the experimental trials to obtain a better quality sheet.

Miyazawa and Szekely et al. [9], developed a 2D model to study the velocity and temperature profile in solid and liquid regions for uncoupled fluid flow and heat transfer. In the liquid pool region, flow is assumed to be laminar while in solid region the flow is assumed to be plastic. The mushy zone was not taken into consideration because of pure aluminium. Sahoo et al. [10-13] developed a 2D model and studied the effect of process parameters such as different inlet temperature (831 K – 941 K) and roll gap (0.8 - 3 mm) for high speed TRC process. The model

was fully coupled with the turbulent form of the Navier Stokes equation with an energy balance equation using ANSYS FLUENT 6.3.16 software. Bondarenko et al. [14] performed simulation on 2D model of TRC at different strip thickness with different lengths of solidification deformation zone (25, 35 and 60 mm) using Finite Element Software ANSYS. Patil et al. [15] studied the effect of turbulence and a rise in viscosity due to phase change. Pressure based solver was used in ANSYS FLUENT 14.0 to solve governing equations by finite volume approach. Rodrigues et al. [16] reported theoretical work on modeling of macro-segregation during twin-roll casting of Al-4wt pct. Cu alloys. They have considered a strip thickness of 8mm where the segregation patterns are more pronounced. Yong Li et al. [17] in a recently published work studied the temperature field distribution in 20 mm thick slab of AA6022 melt, twin roll cast at different rolling speeds, using the commercial software ANSYS 16.0. They predicted that surface quality improves at lower rolling speeds.

Various studies on modelling and simulation of TRC process for different aluminium alloys have been performed till date. But, no significant work has been reported on simulation of vertically twin-roll cast A356 commercial aluminium alloy. In this study, the full geometry of the wedge-shaped region has been taken into consideration for better understanding of the fluid flow, heat transfer and solidification involved during VTRC of A356 aluminium alloy. The simulation was performed using COMSOL Multiphysics 5.4 software. The objective of this study was to optimize the process parameters such as roll gap, roll speed, melt-superheat and convective heat transfer coefficient (h in W/m^2K) at which VTRC can provide a better quality sheet with good quality microstructure having finer grains and near rounded Si morphology. A356 alloy is used in sheet form in the construction of chassis of transportation vehicles.

2. Mathematical Modelling and Numerical Simulation

Computational analysis is a powerful tool to determine the optimal process parameters at which VTRC can provide better quality strips. To simulate fluid flow, RANS equation (Reynolds Average Navier- Stokes) is applied; energy equation with latent heat of solidification model is used for studying the heat transfer and solidification involved during the VTRC process of A356 alloy.

Following assumptions have been taken to simplify the model [10-13].

1. Steady-state flow.
2. A 3D problem is simplified to a 2D problem as the effect of heat transfer, and fluid flow is neglected along the width of rollers.
3. The top surface of the melt pool is considered to be fully developed.
4. Forced convection is dominated over the natural convection, as molten metal is flowing over the moving roll surface.
5. The flow of molten metal is turbulent and incompressible.
6. Molten metal is a Newtonian fluid.

7. A no-slip condition exists between liquid molten metal and the roll/solidified strip surface.
8. Heat transfer is dominated by both conduction and convection mode; heat transfer due to radiation is considered to be negligible.
9. The value of the average heat transfer coefficient is considered to be constant throughout the roll surfaces. Heat transfer coefficient out of the nip point is deemed to be affected by air.
10. The heat caused by plastic deformation and friction is neglected.

Considering steady state condition modified continuity and momentum equations are presented below.

2.1. Continuity equation:

$$\nabla \cdot (\rho u) = 0 \quad (1)$$

Where ρ is the density of molten metal, and u is the velocity vector. It is based on conservation of mass.

2.2. Momentum equation:

RANS equation which is a turbulent form of Navier-Stokes equation is used to model the fluid flow.

$$\rho(u \cdot \nabla)u = -\nabla \cdot [-PI + K] + \rho g + F \quad (2)$$

Where,

$$K = (\mu + \mu_T)(\nabla u + (\nabla u)^T) - \frac{2}{3}(\mu + \mu_T)(\nabla \cdot u)I - \frac{2}{3}\rho kI$$

P is pressure, μ is dynamic viscosity, μ_T is turbulent viscosity, ρg is body force term, F is source term.

$$F = \frac{(1-\alpha)^2}{\alpha^3 + \epsilon} A_{\text{mush}}(u - v_{\text{cast}}) \quad (3)$$

The source term (F) is incorporated to study the flow within the mushy zone. Flow in the mushy region is assumed to be governed by Darcy's law for porous media [18]. It is defined by Enthalpy – Porosity technique to treat the mushy zone as porous media. In the mushy zone, liquid and solid both phases are present in cell volume. The fraction of liquid present in the cell is taken as porosity. Therefore when liquid fraction in a cell is 1, porosity will be 1 and once the complete solidification takes place porosity, and liquid fraction both will become equal to zero. ϵ is a small constant number equal to 0.001, to avoid division by zero. A_{mush} is mushy zone constant whose value varies in between 10^4 - 10^7 , in this model its value is taken as 60,000, A_{mush} signifies for the amplitude of damping of viscosity. v_{cast} is casting velocity.

From equation (3) it is clear when the liquid fraction (α) is equal to 1, Darcy's porosity term (F) will be equal to zero and melt can be treated as complete liquid.

The liquid fraction is calculated as a linear function of temperature.

$$\alpha = \frac{T - T_{\text{solidus}}}{T_{\text{liquidus}} - T_{\text{solidus}}}$$

T = Local temperature

T_L = Liquidus temperature

T_S = Solidus temperature

$$\mu_T = f_{\mu} C_{\mu} \rho \frac{k^2}{\epsilon}$$

μ_T (Turbulent viscosity) depends on the value of k and ϵ which are unknown terms [19]. To calculate these unknowns, two equations are used to calculate the value of each term. k is turbulent kinetic energy; ϵ is turbulent kinetic energy dissipation.

2.3. Turbulent k- ϵ model:

It is a complex problem as two phases (liquid and solid) are present in the same domain. In the molten metal region the viscosity is lower and flow is turbulent, while in the semisolid region (mushy zone) viscosity is relatively higher, and flow is laminar. In this study, low Reynolds k - ϵ turbulence model [19] is used to account for this effect. Low Reynolds k - ϵ turbulence model has an advantage of treating laminar and turbulent flow in the same region without applying additional wall function.

Turbulent kinetic energy equation (k):

$$\rho(u \cdot \nabla)k = \nabla \cdot \left[\left(\mu + \frac{\mu_T}{\sigma_k} \right) \nabla k \right] + P_k - \rho \epsilon + S_k \quad (4)$$

Where,

$$P_k = \mu_T [\nabla u \cdot (\nabla u + (\nabla u)^T)] - \frac{2}{3}(\nabla \cdot u)^2] - \frac{2}{3}\rho k \nabla \cdot u$$

Turbulent kinetic energy dissipation equation (ϵ):

$$\rho(u \cdot \nabla)\epsilon = \nabla \cdot \left[\left(\mu + \frac{\mu_T}{\sigma_{\epsilon}} \right) \nabla \epsilon \right] + C_{\epsilon 1} \frac{\epsilon}{k} P_k - C_{\epsilon 2} f_2 \rho \epsilon^2 / k + S_{\epsilon} \quad (5)$$

σ_k is kinetic energy turbulent Prandtl number, σ_{ϵ} is dissipation turbulent Prandtl number. Empirical damping functions (f_2 , f_{μ}) are used for low Reynolds k - ϵ turbulence model, to reduce the dissipation rate close to the wall.

$$Re_T = \frac{\rho k^2}{\mu \epsilon}$$

(Re_T = Turbulence Reynolds number)

$$f_2 = 1 - 0.3 \exp(-Re_T^2)$$

$$f_{\mu} = \exp[-3.4 / (1 + (Re_T / 50)^2)]$$

(f_{μ} = Damping function)

Different low Reynolds number model has been proposed in the literature. In this study, the recently developed model by Launder and Sharma [20] is applied to account for the coupled fluid flow and solidification.

Table 1 presents the model constants chosen for the present simulation.

Table 1.

Model constant of Launder and Sharma [20]

$C_{\epsilon 1}$	$C_{\epsilon 2}$	C_{μ}	σ_k	σ_{ϵ}
1.44	1.92	0.09	1	1.3

2.4. Energy equation:

A356 is a hypo-eutectic Al alloy; it solidifies over a range of temperature from 886 K (613°C) to 830 K (557°C). Therefore during solidification (Phase transition from liquid to solid), a significant amount of latent heat is released as melt temperature drops below liquidus temperature. The amount of latent heat is function of temperature and liquid fraction [21-22].

$$d_z \rho C_p u \cdot \nabla T + \nabla \cdot q = q_o + d_z Q_p + d_z Q_{vd} \quad (6)$$

Where,

$$q = -d_z K_{eff} \nabla T \quad (\text{Conductive term})$$

$$q_o = h \nabla T \quad (\text{Convective term})$$

$$K_{eff} = K_o + K_t$$

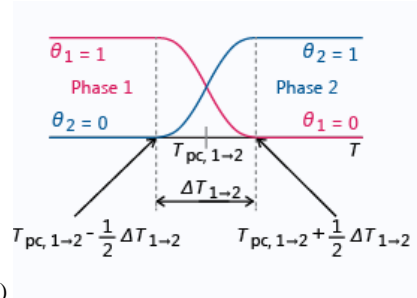
$$\sigma_k \text{ or } (Pr_t) = \mu_t C_p / K_t$$

Where K_{eff} is an effective thermal coefficient for conduction, d_z is the thickness taken as 1; C_p is specific heat capacity. The first term on the LHS of the equation is used to account for latent heat; the second term signifies for conduction. Convection term signifies by q_o , $d_z Q_{vd}$ signifies for mechanical or viscous- dissipation coefficient, other terms of this equation are the source or sink terms.

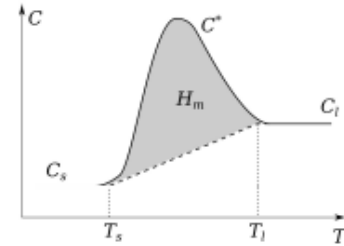
2.5. Latent heat extraction for phase transition:

During phase transition, a significant amount of latent heat is released as mentioned earlier. Latent heat of liquid phase is larger than that of the solid phase. Apparent heat capacity method [23], which is nonlinear temperature-dependent specific heat capacity, is used to calculate local latent heat mentioned in equation 7. The idea of this approach is to decrease the heat capacity (C_p) in the solidifying region in such a way that the extracted energy necessary to solidify the material is equal to latent heat (ΔH).

T_{pc} is phase change temperature. From the Fig.1 (a) presented above, it is clear that the transformation occurs in a temperature interval between $(T_{pc} - \frac{\Delta T}{2})$ and $(T_{pc} + \frac{\Delta T}{2})$. In this interval, the material phase is modelled by a smoothed function α [In Fig.1 (a) this function is represented by θ_1 and θ_2], which represents the phase fraction. If θ_1 shows the liquid phase fraction (α), then θ_2 will represent solid phase fraction ($1 - \alpha$).



a)



b)

Fig.1. (a) Phase transition from liquid to solid. (b) Depicts the increase of latent heat content for melting [28]

Final apparent heat capacity (C_{app}) used in energy equation is given by:

$$\int_{T_{pc} - \frac{\Delta T}{2}}^{T_{pc} + \frac{\Delta T}{2}} C_{app}(T) dT = \int_{T_{pc} - \frac{\Delta T}{2}}^{T_{pc} + \frac{\Delta T}{2}} C(T) dT + H_m \quad (7)$$

$$H_m = L_{1-2} \frac{\partial \alpha}{\partial T} \quad (8)$$

Where, the values of α is given as

$$\alpha = 0, T < T_{solidus}$$

$$\alpha = \frac{T - T_{solidus}}{T_{liquidus} - T_{solidus}}, T_{solidus} < T < T_{liquidus}$$

$$\alpha = 1, T > T_{liquidus}$$

3. VTRC Process Description

Numerical simulation was performed on VTRC where rolls are made of stainless steel material. The liquid A356 alloy is supplied through tundish on to roll surface. The domain is shown below in Fig. 2.

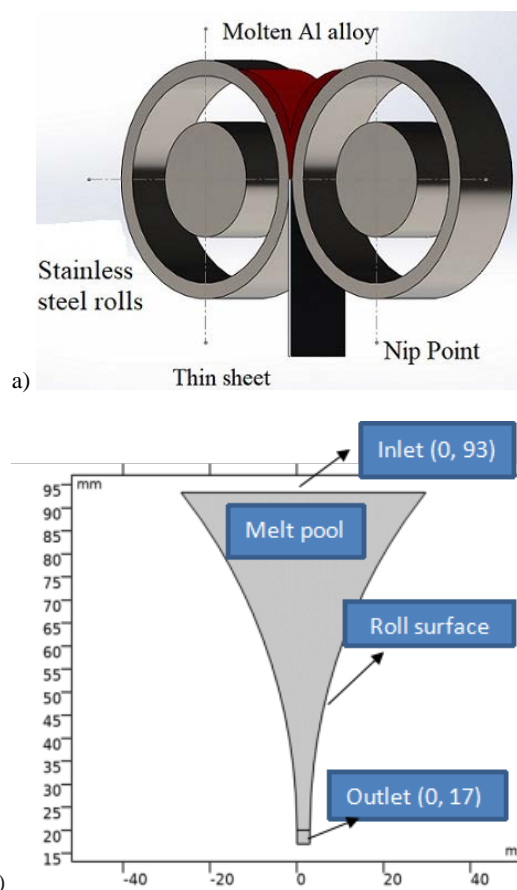


Fig. 2. (a) CAD Model of VTRC, (b) VTRC Model built using COMSOL platform

The CAD model shown in Fig.2 (a) represents the 3D view of VTRC process where two rollers are rotating in opposite direction with same roll speed. The molten metal forms the shells (maroon coloured) at each roll surface when it comes in direct contact with the rolls. Finally, these shells meet at nip point of rolls (smallest distance between two rolls), where the deformation takes place due to high pressure applied by rolls, and a thin sheet of desired thickness is obtained. Fig.2 (b) is the replica of wedge shaped geometry in 2D view which shows different boundaries of VTRC model developed at COMSOL Multiphysics 5.4. Processing parameters used for modelling are listed in Table 2.

Table 2.

Processing parameters used for numerical simulation

Designation	Parameter value	Description
dT	28 K	Temperature transition zone half width
T	1-6 mm	Roll gap
T _{in}	891-922 K	Melt inlet temperature
v _{cast}	0.0477-0.1193 m/s	Roller speed
h _{mold}	2000-8000 W/(m ² *K)	Heat transfer coefficient between roll surface and strip

3.1. Boundary conditions

The boundaries of the model domain are shown in Fig.2 (b). The following casting speeds and thermal boundary conditions are applied.

3.1.1. Inlet condition

The boundary condition in this region consists of the pouring temperature and the inlet velocity of the melt. Different values of inlet temperature have been taken. Some degree of superheat is considered for smooth flow and to avoid sticking.

$$V_x = 0, V_y = u \quad (9)$$

$$T = T_{in} \quad (\text{Inlet temperature}) \quad (10)$$

3.1.2. Roll / Strip interface

A no-slip rotating wall condition is defined in this region. The heat transfer between roll and strip is defined using a heat transfer coefficient (h_{mold}). This value is assumed to remain constant throughout the roll surface from the first point of contact of molten metal against the roll surface to the nip point (smallest distance between two rolls) of the rolls.

$$-n \cdot q = d_z \cdot h_{mold} (T_s - T_R) \quad (11)$$

T_s - Strip surface temperature
 T_R - Roll surface temperature.

Where,

$$q = -d_z K \nabla T \quad (12)$$

K is thermal conductivity, T is temperature, and n denotes the normal direction to the strip surface.

3.1.3. Strip / Free surface interface

In this region, the heat transfer between the strip and free surface is defined using a heat transfer coefficient (h_{air}).

$$-n \cdot q = d_z \cdot h_{air} (T_s - T_o) \quad (13)$$

T_o denotes the ambient temperature.

3.1.4. Outlet

Outlet boundary condition can't be exactly determined since we have no prior information about the variables like velocity, temperature and other parameters.

3.2. Solution techniques

Contrary to the pure metals, A356 which is a hypoeutectic Al alloy undergoes a broad temperature transition zone ($\sim 56^\circ\text{C}$). VTRC model contains three zones of different phases, complete liquid region, mushy zone (consist both the liquid and solid phase) and solid region, as shown in Fig.3. To account for heat transfer, fluid flow and phase transformation (from liquid to solid) extra-fine mesh is generated.

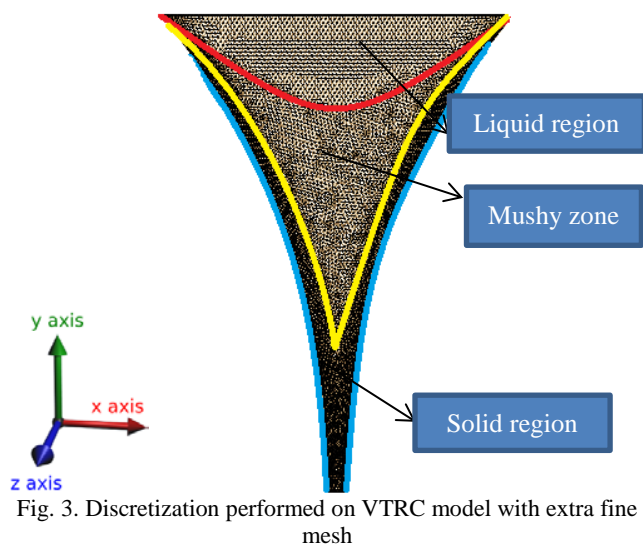


Fig. 3. Discretization performed on VTRC model with extra fine mesh

The conservation equations were discretized and solved using the COMSOL Multiphysics 5.4 software. This software uses (FEM) Finite Element approach [24] to solve the above mentioned partial differential equations.

To understand the convergence behavior of this problem, it is necessary to examine the governing equations involved in the finite-element method. The governing equations are applied to each element producing a global system of nonlinear algebraic equations. The highly non-linear aspects of the governing equations for present turbulent flow field made the solution more prone to instability. Use of $k-\epsilon$ turbulence model contributes to improve stability. This is done by increasing the effective viscosity, thereby increasing the importance of the linear terms and substantially reducing the grid Reynolds number. Maximum and minimum element size of the generated mesh is 0.732 mm and 0.00845 mm. Convergence is attained only when relative error is smaller. Table 3 lists the thermo-physical properties used for A356 alloy (Al-7.5%Si-0.3%Mg).

Table 3.

Thermo-physical properties of A356 aluminium alloy [25]

Properties	Value
Liquidus temperature (T_L)	613°C (886 K)
Eutectic temperature (T_S)	557°C (830 K)
Density (liquidus point) (ρ_L)	2495 kg/m ³
Density (solidus point) (ρ_S)	2680 kg/m ³
Specific heat (C_{ps})	900 J/kg·K
Specific heat (C_{pl})	1160 J/kg·K
Latent heat (L)	397,700 J/kg
Viscosity (μ)	0.00113 kg/m·sec
Thermal conductivity	160 W/m.K

4. Experimental

The as-cast sample of 3 mm thickness was prepared by permanent-mold casting. The ingots of commercial A356 alloy were melted in Kanthal muffle furnace at a temperature of 625 °C with an accuracy of ± 5 °C. Mold was kept at room temperature [26]. A total of 2Kg of melt was processed.

The VTRC samples were prepared by re-melting the A356 aluminium alloy in a crucible in a Kanthal muffle furnace at a temperature of 625° C. The melt was poured directly into the tundish through a nozzle into the wedge-shaped region formed by the counter-rotating rolls of the VTRC setup. Solidification takes place as the superheated liquid metal comes in contact with the moving rolls. A thin solidified shell is formed on the surface of each roll. The thickness of the solidified shells increases with continuous heat extraction. Finally, the two solidified shells meet at the nip point (minimum distance between two rolls) of the rolls and the alloy exits from the VTRC setup in the form of solidified strip. A considerable amount of pressure is applied at nip point by the rolls and a thin sheet of 3mm thickness is formed at the end of this process. The schematic diagram of VTRC set-up is shown in Fig.4 where the rolls were made of stainless steel provided with water cooling system. A roll speed controller device was attached with the setup to maintain the roll speed. Rolls had 22.5 cm diameter of which 1.5 cm thick outer ring was made of stainless steel and were 25 cm in width.

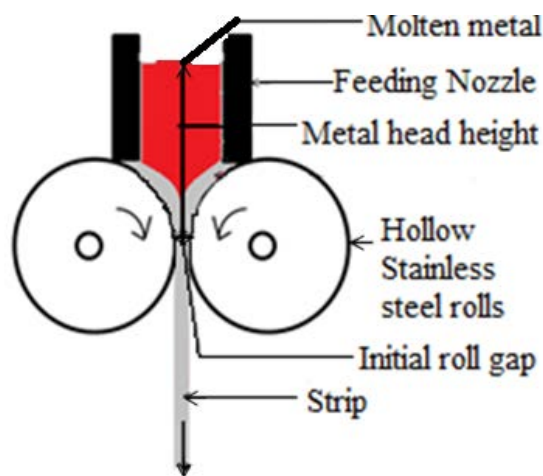


Fig. 4. Schematics diagram of VTRC set-up

After completing the alloy preparation using both the casting routes the samples were sectioned from the parent parts and prepared for metallographic examination by the usual grinding and polishing route. The grain size was analysed by quantitative metallographic analysis using an optical microscope and ImageJ 1.x software was used for further analysis. FESEM (Field Emission Scanning Electron Microscope) equipped with a back-scattered electron (BSE) and a secondary electron (SE) detector [27] was used to characterize the samples to study the Si morphology in cast samples.

5. Results and discussion

5.1 Modelling and simulation:

5.1.1 Effect of different roll speeds

In order to study the effect of different roll speeds on cast A356 alloy sheets, simulation has been performed at 0.0477 m/s, 0.0955 m/s and 0.1193 m/s roll speeds, keeping the other parameters constant, such as inlet temperature of 886 K and roll gap of 3 mm. Fig. 5 presents the results of the simulation.

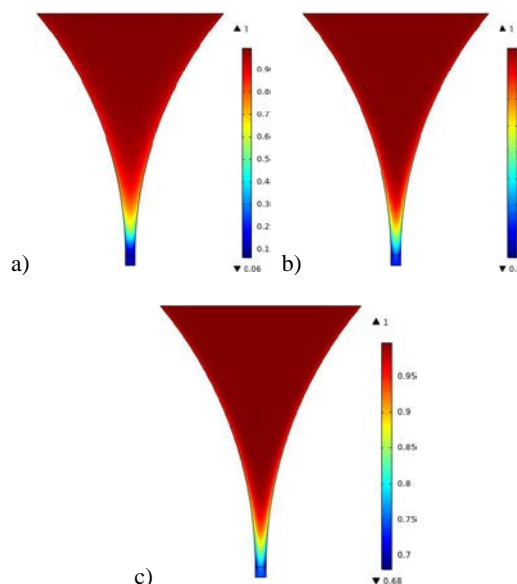


Fig. 5. Liquid Fraction profile at different roll speeds (a) 0.0477 m/s; (b) 0.0955 m/s; (c) 0.1193 m/s

It is observed that, as the roll speed is increasing the temperature and liquid fraction at the nip point is increasing. This is due to the fact that the higher roll speed causes shifts in the freezing point of the molten alloy towards the exit point. Thus at very high roll speed the material will not solidify completely before reaching to the nip point resulting in ineffective plastic deformation. Thus chances of getting porosities in the processed sheets are increased. Therefore a lower roll speed of 0.0477 cm/s is predicted to be suitable for processing.

5.1.2. Effect of different roll gaps

Roll gap is another important factor that not only affects the final sheet thickness but also affects the sheet formation possibility. For a sheet to form at the end of the process, the roll gap should be such that a small amount of molten metal remains in the region just above the nip point (the shortest distance between two rolls) of the rolls. The simulation has been performed at different roll gaps (which corresponds to thickness of the sheet) of 1 mm, 3 mm and 6 mm keeping the other parameters constant, such as inlet temperature of 886 K and roll speed of 4.77 cm/s to cast A356 sheets. The variation of temperature profiles as function of different roll gaps is shown in Fig.6.

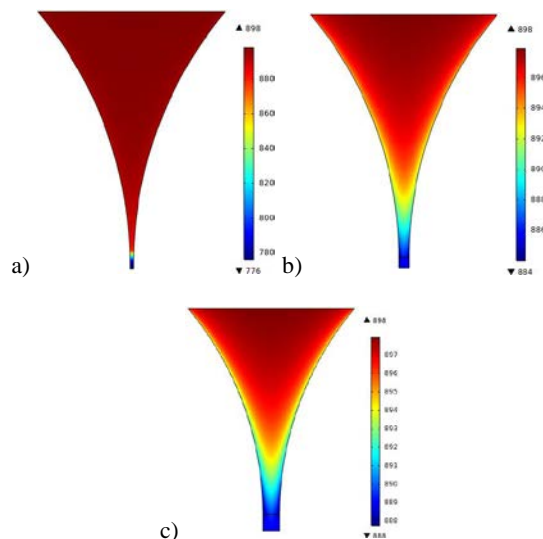


Fig. 6. Temperature profile at different roll gap (a) $t = 1$ mm (b) $t = 3$ mm (c) $t = 6$ mm

It is clear that as the roll gap is increasing, the temperature and liquid fraction at the nip point is increasing. Liquid fraction is 0, 0.5 and 0.61 at roll gap of 1 mm, 3 mm and 6 mm respectively. This can be attributed to the flow rate which depends on the area of the passage as well as melts velocity. Thus, as the area is increasing the flow rate of liquid molten metal is increasing. The molten metal will flow down at a faster rate at high roll gap. This leads to less residence time for molten metal in contact with the roll surface which affects the amount of heat extracted. Presence of less liquid in the roll gap region also reduces the turbulence or back flow of the liquid and thus lessens the solute segregation [16]. As it has already been mentioned that it is preferred to cast thin sheets (low roll gap) of an alloy with wide solidification range to avoid segregation and surface bleed or there must be some additional cooling techniques provided to cast thick sheets of an alloy with wide solidification range. Some methods to provide additional cooling such as electromagnetic oscillation field, Magnetic stirring [2, 17] and pulse electric current field have been reported to control the macro-segregation. Therefore VTRC at low roll gap is found to be preferable for reducing the segregation and porosity defects.

5.1.3 Effect of different melt superheats

Melt superheat is one of the most crucial parameters for the VTRC process. An accurate inlet temperature needs to be regulated accurately to obtain well-formed sheets at the end of the process. For example, a high superheated molten metal will allow the melt to flow like fluid from the wedge-shaped region formed in between the rollers. To determine the appropriate melt pouring temperature, simulation has been performed at 5°C, 12°C, 24°C and 36°C superheat above the liquidus temperature keeping the other parameters constant, such as roll gap of 3 mm and roll speed of 0.0477 m/s to cast A356 aluminium alloy sheet. The simulation results have been shown in Fig. 7.

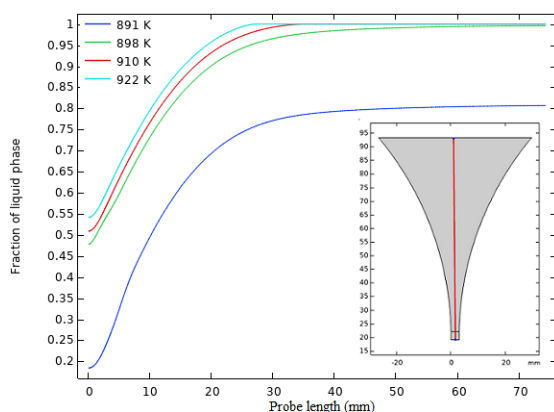


Fig. 7. Liquid fraction profile at different inlet temperatures along the probe length (marked as straight line at the centre of geometry).

From the obtained simulation result, it is clear that on increasing pouring temperature, the temperature and liquid fraction at outlet of the nip point is increasing. The liquid fraction is increasing above 0.5 at 922 K which means molten metal will flow down from the wedge shaped region with no sheet formation at the end of procedure. It is seen from Fig.7, that as the melt superheat is increasing, the mushy zone is shifting towards the nip point, and the amount of solid fraction in the wedge-shaped region is decreasing. This will increase the chances of getting surface bleeds, as this defect happens because of incomplete solidification before reaching to the nip point. At 891 K inlet temperature the liquid fraction obtained is 0.14, which means a high amount of solid fraction remains in the wedge-shaped region. Thus a melt superheat of 5-12° C is preferable for A356 alloy for VTRC in the set up proposed.

5.1.4. Effect of convective heat transfer coefficient

To study the effect of convective-heat transfer coefficient, simulation has been performed at different values of h_{mold} , keeping the other parameters such as inlet temperature of 886 K and roll speed of 0.0477 m/s and the roll gap of 3 mm constant to cast A356 sheets. Fig. 8 presents the results of simulation.

As the value of h_{mold} is increasing from 2000 - 8000 W/m²K, the temperature at the exit of roll is decreasing from 890 – 878 K. Also liquid fraction decreases from 0.75 to 0.06 as the heat extraction from the roll surface increases. Increasing convective heat transfer coefficient will lead to the reduction in surface bleeds defects, as the melt will solidify completely before reaching to the nip point at high value of convective heat transfer coefficient.

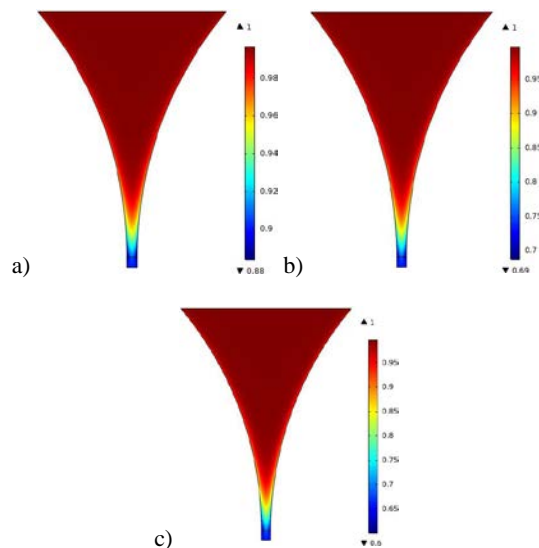


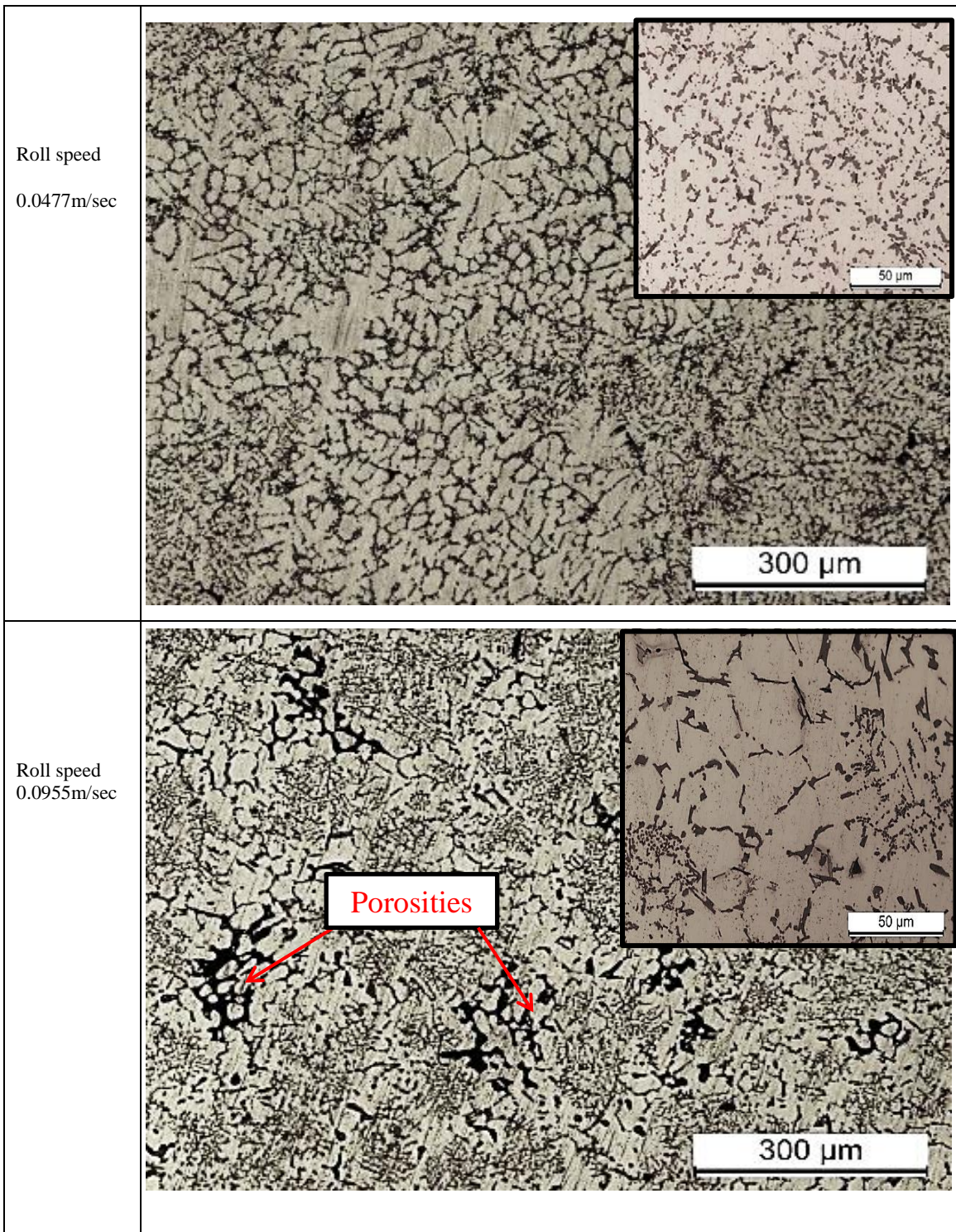
Fig. 8. Liquid fraction at different heat transfer coefficient (a) $h_{\text{mold}} = 2000 \text{ W/m}^2\text{K}$, (b) $h_{\text{mold}} = 6000 \text{ W/m}^2\text{K}$, (c) $h_{\text{mold}} = 8000 \text{ W/m}^2\text{K}$

It is possible to cast an alloy which possesses wide freezing range by using roll material of high thermal conductivity like water cooled stainless steel rolls.

5. 2. Experimental

5.2.1. Microstructural analysis of VTRC cast alloys

The developed computational fluid dynamics (CFD) model for different processing parameters was validated by using the results obtained from experimental analysis. Fig.9 presents the microstructures for sheets obtained by performing the experiments at 0.0477 m/s, 0.0955 m/s and 0.1193 m/s roll speeds while keeping the other parameters constant. Pouring temperature, roll gap and heat transfer coefficient were held at $T_{\text{in}} = 898 \text{ K}$, $t = 3 \text{ mm}$, $h_{\text{mold}} = 8000 \text{ W/m}^2\text{K}$ respectively. Samples for metallographic analysis were selected from near the top surface of the cast sheets for microstructural comparison at different roll speeds. It is expected that in this case the structure would also show any defect formation tendencies.



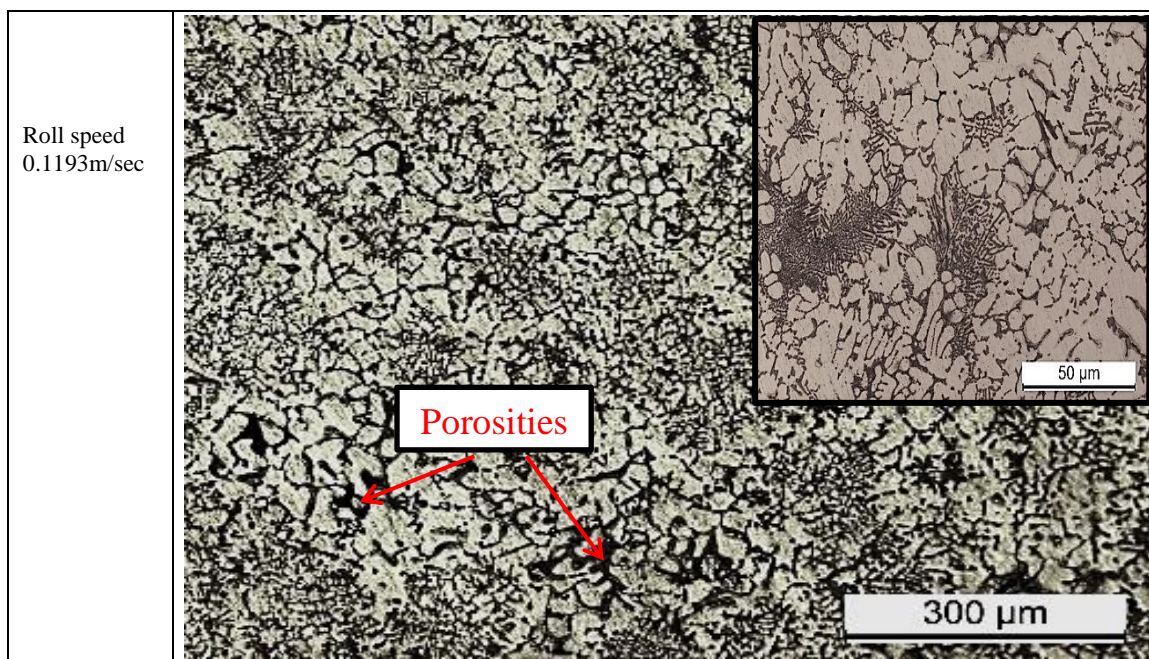


Fig. 9. Microstructures obtained at different roll speeds for validation of simulated results

The bright phases present in the microstructure are the primary α -Al phase while the dark phase shows the presence of eutectic phase. At 0.0477 m/s roll speed, a microstructure with very fine equiaxed particles and much smaller particles of the eutectic Si is observed. As the roll speed is increasing the residence time for molten metal in contact with the roll surfaces is decreasing. This results in low solid fraction in between the roll gap and consequently the amount of effective roll deformation of the forming sheet is decreasing with an increase in roll speed. At 0.0955 m/s roll speed, some porosity with coarser grains of primary α -Al dendrites is observed. Also the finer particles of eutectic-Si obtained at 0.0477 m/s has changed in to plate like morphology at 0.0955 cm/s roll speed. At 0.1193 m/s roll speed, the number of porosities is increased with complete acicular (plate-like) morphology of eutectic-Si particles and much coarser particles of primary α -Al dendrites. Also because of ineffective plastic deformation the microstructure is not uniformly distributed, some bunches of eutectic-Si phase can be observed at 0.1193 m/s roll speed. A variation in the grain size in the cast sheet is seen at higher roll speeds. It can be inferred from these experimental results that the amount of plastic deformation will change effectively at different roll speed during VTRC process. Thus, 0.0477 m/s is most preferred roll speed for VTRC of A356 Al alloy in this study. The suitability of the lower rolling speed is in line with those predicted by Li et. al [17]. At this roll speed, the residence time of melt inside the pool is large, causing more heat extraction from the solidifying strip. Most of the regions of molten metal solidify before reaching the nip point and an adequate amount of plastic deformation is experienced, which results in fragmentation of coarse-sized eutectic-Si particles and provide more refined microstructure with no/minimum porosities.

5.2.2. Comparison of VTRC alloy cast under optimum conditions with die-cast alloy

For further studying the nature of the Si particles, FESEM characterization was done. For comparison the Si particles obtained in die cast sample of the same alloy is also presented. Fig.10 presents the FESEM micrographs of the sheet cast at optimum processing parameters and that of die cast sample of A356 alloy.

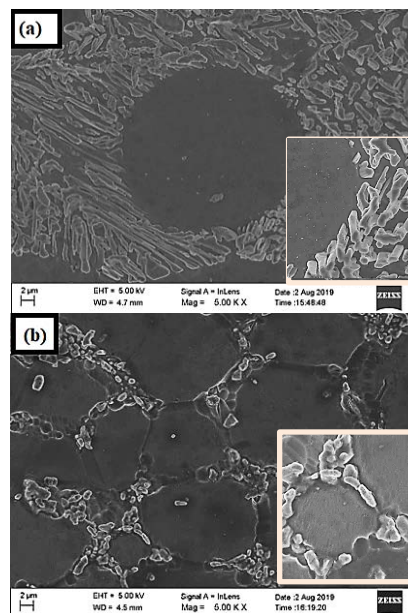


Fig.10. FESEM microstructures of (a) die cast sample and (b) VTRC sample

The bright regions here show the presence of eutectic Si, while dark region represents the primary α -Al matrix in Fig.10. The as-cast sample consists of acicular plate like morphology of eutectic-Si particles, while the VTRC processed sample shows the broken particles of eutectic Si. This can be attributed to the high cooling rate and plastic deformation applied by rolls resulting in the modification of eutectic-Si morphology during VTRC process. Much smaller particles of eutectic-Si are observed. Fig.11 presents the average eutectic Si length and secondary dendrite arm spacing for the die cast and VTRC samples prepared under optimum processing parameters.

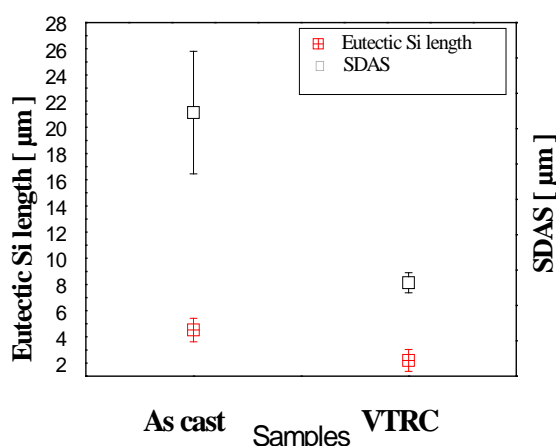


Fig. 11. SDAS and Eutectic-Si length comparison for as-cast and VTRC sample

Equation that relates cooling rate and SDAS is presented below:

$$SDAS = C \left[\frac{T_1 - T_e}{\dot{T}} \right]^{\frac{1}{3}} \quad (14)$$

Where, T_1 is liquidus temperature, T_e is eutectic temperature, C is constant whose value depends upon a particular alloy, SDAS is in μm , \dot{T} is cooling rate in $^{\circ}\text{C}/\text{sec}$.

The average secondary dendritic arm spacing (SDAS) achieved from VTRC sample is around $8\mu\text{m}$, while for as-cast sample it is around $22\pm 2\mu\text{m}$. The line intercept method was adopted to measure the dendritic arm spacing at different locations. Reduced dendritic arm spacing leads to homogenization of VTRC processed sample.

The above mentioned equation suggests that the cooling rate is inversely proportional to the SDAS value [28-29]. Thus the higher cooling rate during VTRC process is expected to lower the values of SDAS compared to the as-cast sample. The finer structure also showed higher average hardness in the VTRC sample of 81.6 VHN as compared to an average hardness of 68.6 VHN for die cast samples. This points out to some additional mechanisms contributing to the hardness other than the Hall-Petch.

6. Conclusions

1. Modelling and numerical simulation of VTRC process for A356 alloy was performed in order to optimize the processing parameters such as inlet temperature, roll gap, heat transfer coefficient, and roll speed.
2. A 2D mathematical model was developed to analyse the fluid flow and heat transfer involved in the process. The emphasis was on optimization of processing parameters in order to obtain a better quality sheet.
3. The modelling results showed that all the parameters selected affect the fluid flow, heat transfer and solidification during complex VTRC process.
4. Melt superheat of $5-12^{\circ}\text{C}$ at 0.0477 m/s roll speed for 3 mm sheet thickness is found to be the preferred parameters for vertical twin-roll casting of A356 alloy in the set up used.
5. At higher roll speeds the Si particles retained the acicular structure and also defects were seen on the surface of the cast strips.
6. The microstructure of VTRC processed sample under optimum processing parameters revealed finer eutectic Si particles compared with the die cast sample. Also, the hardness value for VTRC sample (81.6 VHN) is greater than the as cast sample (68.6 VHN). The VTRC sample showed lower SDAS value ($8.13\mu\text{m}$) when compared it with as cast sample ($21.12\mu\text{m}$).

References

- [1] Hong, S., Kim, S., Lee, J., Kwon, Y., Lee, Y. & Lee, J. (2007). Effect of microstructural variables on tensile behaviour of A356 cast aluminium alloy. *Materials Science and Technology*. 23(7), 810-814. DOI: 10.1179/174328407x185866.
- [2] Ordóñez, S., Bustos, O. & Colás, R. (2009). Thermal and Microstructural analysis of an A356 aluminium alloy solidified under the effect of magnetic stirring. *International Journal of Metalcasting*. 3(3), 37-41. DOI:10.1007/bf03355451.
- [3] Haga, T., Takahashi, K., Ikawa, M., & Watari, H. (2003). A vertical-type twin roll caster for aluminium alloy strips. *Journal of Materials Processing Technology*. 140 (1-3), 610-615. DOI: 10.1016/s0924-0136(03)00835-5.
- [4] Yuan, H., Li, J., Cai, D., Yang, Q. & Liu, W. (2007). Quantitative Analysis of Texture Evolution of Direct Chill Cast and Continuous Cast AA 1100 Aluminum Alloys during Cold Rolling. *Materials Transactions*. 48(7), 1886-1890. DOI: 10.2320/matertrans.mra2007023.
- [5] Zhao, Y. M., Liu, W. C. & Morris, J.G. (2003). Comparison of texture evolution during cold rolling between direct chill and continuous cast aluminium alloy 5052. *Materials Science and Technology*. 19(10), 1379-1385. DOI: 10.1179/026708303225008004.
- [6] Slámová, M., Karlík M, Robaut, F., Sláma, P. & Véron, M. (2002). Differences in microstructure and texture of Al-Mg sheets produced by twin-roll continuous casting and by

- direct-chill casting. *Materials Characterization*. 49(3), 231-240. DOI: 10.1016/s1044-5803(03)00011-1.
- [7] Maleki, A., Taherizadeh, A. & Hosseini, N. (2017). Twin Roll Casting of Steels: An Overview. *ISIJ International*. 57(1), 1-14. DOI: 10.2355/isijinternational.isijint-2016-502.
- [8] Barekar, N.S. & Dhindaw, B.K. (2014). Twin-Roll Casting of Aluminum Alloys – An Overview. *Materials and Manufacturing Processes*. 29(6), 651-661. DOI: 10.1080/10426914.2014.912307.
- [9] Miyazawa, K. & Szekely, J. (1981). A mathematical model of the splat cooling process using the twin-roll technique. *Metallurgical Transactions A*. 12(6), 1047-1057. DOI: 10.1007/bf02643486.
- [10] Sahoo, S. & Ghosh, S. (2013). Heat Transfer, Solidification, and Microstructural Evolution in Al-33Cu Alloy during the Starting of Twin Roll Strip Casting. *Steel Research International*. 85(2), 207-218. DOI: 10.1002/srin.201200262.
- [11] Sahoo, S. (2016). Review on Vertical Twin-Roll Strip Casting: A Key Technology for Quality Strips. *Journal of Metallurgy*. 2016, 1-13. DOI: 10.1155/2016/1038950.
- [12] Sahoo, S., Kumar, A., Dhindaw, B.K. & Ghosh, S. (2012). Modeling and Experimental Validation of Rapid Cooling and Solidification during High-Speed Twin-Roll Strip Casting of Al-33 wt pct Cu. *Metallurgical and Materials Transactions B*. 43(4), 915-924. DOI: 10.1007/s11663-012-9659-x.
- [13] Sahoo, S. (2015). Effect of process parameters on solidification of Al-33Cu strip in high speed twin roll strip casting- A numerical study. IOP Conference Series: Materials Science and Engineering. 75, 012013. DOI: 10.1088/1757-899x/75/1/012013.
- [14] Bondarenko, S., Stolbchenko, M., Schaper, M. & Grydin, O. (2018). Numerical Analysis of Twin-Roll Casting of Strips with Profiled Cross-Section. *Materials Research*. 21 (4). DOI:10.1590/1980-5373-mr-2017-1098.
- [15] Patil, Y.G. & Shukla, A.K. (2019). Numerical Simulation of the Effect of Process Parameters on Cooling Rate and Secondary Dendrite Arm Spacing in High-Speed Twin Roll Strip Casting of Al-15 wt % Cu Alloy. *Journal of Heat Transfer*. 141(10). DOI:10.1115/1.4044108.
- [16] Rodrigues, C.M., Ludwig, A., Wu, M., Kharicha, A. & Vakhrushev, A. (2019). A comprehensive analysis of Macrosegregation formation during twin-roll casting. *Metallurgical and Materials Transactions B*. 50(3), 1334-1350. DOI:10.1007/s11663-019-01527-x.
- [17] Li, Y., He, C., Li, J., Wang, Z., Wu, D. & Xu, G. (2020). A novel approach to improve the microstructure and mechanical properties of al-mg-si aluminum alloys during twin-roll casting. *Materials*. 13(7), 1713. DOI:10.3390/ma13071713.
- [18] Wang, B., Zhang, J., Fan, J., Zhao, S., Ren, S. & Chou, K. (2010). Modelling of melt flow and solidification in the twin-roll strip casting process. *Steel research international*. 80(3), 218-222. DOI:10.1002/srin.201090074.
- [19] Launder, B. & Spalding, D. (1974). The numerical computation of turbulent flows. *Computer Methods in Applied Mechanics And Engineering*. 3(2), 269-289. DOI: 10.1016/0045-7825(74)90029-2.
- [20] Launder, B. & Sharma, B. (1974). Application of the energy-dissipation model of turbulence to the calculation of flow near a spinning disc. *Letters in Heat and Mass Transfer*. 1(2), 131-137. DOI:10.1016/0094-4548(74)90150-7.
- [21] Voller, V., Brent, A. & Prakash, C. (1989). The modelling of heat, mass and solute transport in solidification systems. *International Journal of Heat and Mass Transfer*. 32(9), 1719-1731. DOI:10.1016/0017-9310(89)90054-9.
- [22] Voller, V. & Prakash, C. (1987). A fixed grid numerical modelling methodology for convection-diffusion mushy region phase-change problems. *International Journal Of Heat And Mass Transfer*. 30(8), 1709-1719. DOI: 10.1016/0017-9310(87)90317-6.
- [23] Yao, M. & Chait, A. (1993). An alternative formulation of the apparent heat capacity method for phase-change problems. *Numerical Heat Transfer, Part B: Fundamentals*. 24(3), 279-300. DOI:10.1080/10407799308955894.
- [24] Thomas, B.G. & Najjar, F.M. (1991). Finite element modelling of turbulent fluid flow and heat transfer in continuous casting. *Applied Mathematical Modelling*. 15(5), 226-243. DOI:10.1016/0307-904x(91)90001-6.
- [25] Das, P., Samanta, S.K., Chattopadhyay, H., Sharma, B.B. & Dutta, P. (2013). Eulerian two-phase flow simulation and experimental validation of semisolid slurry generation process using cooling slope. *Materials Science and Technology*. 29(1), 83-92. DOI: 10.1179/1743284712y.0000000075.
- [26] Permanent Mold Casting of Aluminum Alloys. (2018). *Aluminum Science and Technology*. 209-231. DOI 10.31399/asm.hb.v02a.a0006513
- [27] Scanning electron microscopy. (2005). *Electron Microprobe Analysis and Scanning Electron Microscopy in Geology*. 41-75. DOI:10.1017/cbo9780511610561.005.
- [28] Murthy, I. N. & Rao, J. B. (2017). Evaluation of the microstructure, secondary dendrite arm spacing, and mechanical properties of Al-Si alloy castings made in sand and Fe-Cr slag molds. *International Journal of Minerals, Metallurgy, and Materials*. 24(7), 784-793. DOI: 10.1007/s12613-017-1462-x.
- [29] Cho, J.-I., Kim, C.-W., Kim, Y.-C., Choi, S.-W. & Kang, C.-S. (2012). The Relationship between Dendrite Arm Spacing and Cooling Rate of Al-Si Casting Alloys in High Pressure Die Casting. ICAA13: 13th International Conference on Aluminum Alloys, 1493-1498. DOI:10.1002/9781118495292.ch226.